Simple thermal decomposition route to size-tunable cobalt(II) oxide and cobalt(II,III) oxide nanoparticles for nanoelectronic devices

Nguyen Thi Phuong Loan[1,*], *Hsin-Yi Ma*[2], *Hsiao-Yi Lee*[3]

[1]Faculty of Fundamental 2, Posts and Telecommunications Institute of Technology, Ho Chi Minh City, Vietnam
[2]Department of Industrial Engineering and Management, Minghsin University of Science and Technology, Hsinchu, Taiwan
[3]Department of Electrical Engineering, National Kaohsiung University of Science and Technology, Kaohsiung, Taiwan

*Corresponding Author: Nguyen Thi Phuong Loan (email: ntploan@ptithcm.edu.vn)
(Received: 24-September-2025; accepted: 21-November-2025; published: 31-December-2025)
http://dx.doi.org/10.55579/jaec.202594.518

Abstract. *The present article a simple and controllable method for synthesizing cobalt oxide nanoparticles (CoO and Co_3O_4) with adjustable particle dimensions and morphologies. Cobalt glycerolate was first obtained by refluxing cobalt nitrate and glycerol for four hours, then thermally decomposed at 450–650°C under a mixed oxygen/nitrogen atmosphere for one hour to produce cobalt oxide nanoparticles. The structural phases and crystallite sizes were investigated using X-ray diffraction (XRD) and calculated via the Scherrer equation, while investigated and scanning electron microscopic examination (TEM and SEM) confirmed particle shape, size distribution, and surface uniformity. By varying the decomposition temperature, both particle size and phase composition were effectively controlled—lower temperatures favoring smaller CoO nanoparticles and higher temperatures producing larger, well-crystallized Co_3O_4 particles. The resulting nanoparticles exhibit uniform morphology, high crystallinity, and controllable dimensions, making them suitable for diverse applications in lithium-ion batteries, chemical sensors, and nanoelectronic devices. This straightforward synthesis strategy offers an efficient and scalable route for tailoring cobalt oxide nanomaterials with desirable structural and functional properties.*

Keywords: *Nanoparticles; cobalt oxides; glycerolate; heating breakdown; nanocrystals.*

1. Introduction

Cobalt-based nanoparticles have attracted a lot of attention in recent years owing to their versatile and adjustable physicochemical characteristics, which make them suitable for a broad range of technological purposes [1–3]. Their unique electrochemical, magnetic, and catalytic characteristics stem from cobalt's variable oxidation states and strong spin–orbit coupling, enabling the design of multifunctional nanomaterials for energy storage, sensing, catalysis, and magnetic devices. Among cobalt oxides, CoO and Co_3O_4 represent two particularly important phases [4–6], each offering distinct structural

and functional attributes that lend themselves to different industrial and scientific uses [7–9].

CoO is widely used as a precursor for cobalt salts in the chemical industry and as a blue coloring agent in glass and ceramics [10]. Beyond its decorative use, its antiferromagnetic nature and narrow bandgap make CoO nanoparticles valuable components in nanocomposite materials, where they can influence magnetic coupling, electron transport, and optical behavior [11]. In contrast, Co_3O_4 exhibits a normal spinel crystal structure with mixed Co^{2+} and Co^{3+} valence states, conferring high redox activity and structural stability. Owing to these features, Co_3O_4 has found versatile applications in heterogeneous catalysis [12], gas sensors [13], lithium-ion batteries, and supercapacitors [14]. In particular, its ability to undergo reversible redox transitions between Co^{2+} and Co^{3+} enables efficient charge transfer processes, which are critical in electrochemical energy storage and catalytic oxidation reactions [15–17].

Furthermore, cobalt oxide nanoparticles are frequently employed as precursors in various solid-state synthesis processes [18, 19]. Their high surface area and well-defined oxygen stoichiometry significantly accelerate reaction kinetics, allowing for reduced calcination temperatures and shorter processing times compared with bulk materials, which often require prolonged heating due to limited diffusion rates. This makes nanoscale cobalt oxides highly desirable intermediates for fabricating advanced oxide materials with controlled morphology and stoichiometry [20–22].

Numerous synthetic approaches have been created for preparing cobalt oxide nanoparticles with controlled particle size, morphology, and crystallinity. CoO nanoparticles have been successfully produced through liquid-phase synthesis, alcohol-mediated thermal decomposition of metal oleates, and high-energy ball milling [23]. Likewise, Co_3O_4 nanoparticles have been synthesized using vapor-phase routes, solid–liquid methods, polymer combustion, apoferritin cavity templating, and nitric oxide-mediated thermal decomposition of cobalt nitrates [24]. Although these methods provide flexibility in tuning particle characteristics, many of them are constrained by high process complexity, elevated costs, and limited scalability. Moreover, the resulting particles often exhibit broad size distributions, irregular morphologies, or residual organic impurities, which can hinder reproducibility and restrict their practical applicability in real-world devices and catalytic systems [25].

In the present study, we propose a straightforward, economical, and reproducible approach to synthesize CoO and Co_3O_4 nanoparticles with adjustable particle sizes, addressing the limitations of conventional synthesis techniques that often require complex procedures or expensive reagents. The proposed method utilizes cobalt glycerolate as an intermediate precursor, prepared through a controlled reflux reaction between cobalt nitrate and glycerol. This organic–inorganic coordination compound serves as a uniform source of cobalt and carbon, allowing for precise heating conversion into oxide phases. Subsequent thermally breaking down of the cobalt glycerolate under a regulated oxygen/nitrogen environment yields phase-pure CoO or Co_3O_4 nanoparticles, depending on the annealing temperature and ambient composition [26–28].

The resulting nanoparticles were thoroughly characterized to establish the connection among synthesizing parameters and material properties. X-ray diffraction (XRD) study was used for determining crystalline phase composition and mean crystallite dimension, computed utilizing the Scherrer formula. Morphological and dimensional verification was done through scanning electron microscopy (SEM) and transmitting electron microscopic examination (TEM), which confirmed the uniformity and nanoscale dimensions of the synthesized particles. Notably, the particle size could be precisely tuned just by adjusting the decomposition temperature, eliminating the need for additional surfactants, capping agents, or post-synthesis treatments [29].

This temperature-dependent synthesis strategy provides a scalable and environmentally benign route to producing cobalt oxide nanoparticles with controllable structure and morphology [30, 31]. The method's reproducibility and material uniformity make it particularly suit-

able for applications in energy storage, gas sensing, and heterogeneous catalysis—fields where particle size and phase purity critically influence electrochemical and catalytic performance. Moreover, by utilizing inexpensive precursors and a straightforward synthesis setup, this approach bridges the gap between laboratory-scale nanoparticle fabrication and industrial-level production, offering a practical pathway toward high-quality cobalt oxide nanomaterials for advanced functional applications.

2. Experimental

The initial stage involved reacting water-free glycerol with cobalt nitrate underneath reflux for four hours to create cobalt glycerolate. Following the thermal process, distilled water was added to the solution. After filtering out of suspension, the solid stage that had developed was allowed to air dry. X-Ray diffraction (XRD), component evaluation, atomic absorption spectroscopy (AAS), and X-Ray photoelectron spectroscopy (XPS) were used to describe the outcome and verify the synthesis of cobalt glycerolate. The dried cobalt glycerolate was placed in a tube furnace under a flowing atmosphere of nitrogen or oxygen. Specimens were heated to target temperatures of 450, 500, 550, 600, or 650^{o}C, held for 1h, and then cooled naturally to room temperature. Following that, XRD and SEM were utilized to examine the resultant specimens. Cobalt(II) nitrate hexahydrate ($Co(NO_3)_26H_2O$, $\geq$ 99%) and anhydrous glycerol ($C_3H_8O_3$, $\geq$ 99%) were used as starting materials. Distilled water was used as a solvent. Nitrogen (99.9999%) and oxygen (99.5%) gases were supplied by SIAD, Czech Republic. All chemicals were used as received without further purification [32–35].

An analyzing device was employed for combustible elemental examination (CHNS–O). The device uses the traditional burning concept to transform the specimen components into basic gases (CO_2, H_2O, and N_2) when using CHN mode, which is the most reliable and interference-free option. Automatic burning and decrease, product gas mixing, separating, and detecting are all carried out by the PE 2400 analyzer. CHN assessment precision is higher than 0.30% abs. The spectral measuring device Spectr AA880 (Varian) was used to carry out Atomic Absorption Spectroscopy in order to ascertain the cobalt content [36–38].

The ESCAProbeP spectral measuring device was used for performing superior resolution X-ray photoelectron spectroscopic device (XPS) with a monochromatic aluminum X-ray radiation source. Each component underwent a broad-scan examination. The separate component concentrations from the research hue ranges were evaluated using comparative sensitivity coefficients. The specimen was fastened to an elevated-purity silver bar conducting container [39].

Utilizing a Tescan Lyra dual beam microscope equipped with a FEG electron source, SEM was utilized for examining the shape of the nanoparticles. Throughout measuring purposes, the specimens were put on a carbon conducting tape. A 10 kV electron beam was used for SEM observations.

A 6 μl drop of the investigated solution was applied to a carbon-covered copper grid to create the specimens for transmitting electron microscopy. Any surplus solution was subsequently eliminated and Whatman filtering paper was used to dry the grids. The JEOL JEM-1010 transmitting electron microscope was used to view specimens. AnalySIS v.2.0 software was used to analyze the images captured by the SIS MegaView III digital camera [40].

3. Results and discussion

Cobalt glycerolate was thermally decomposed under a carefully controlled oxygen/nitrogen atmosphere to synthesize CoO and Co_3o_4 nanoparticles. X-ray diffraction (XRD) analysis revealed that cobalt glycerolate possesses an amorphous or nanostructured nature, as indicated by the broad diffraction maxima observed at $2\theta = 10.2^o, 33.8^o$ and 60^o. These broad peaks suggest the absence of long-range crystallinity and the presence of nanoscale order within the precursor. To confirm the material's composition and stoichiometry, since the XRD patterns

alone were not sufficient for phase identification, the specimen was further examined through compositional analysis and atomic absorption spectroscopy (AAS). The results of these investigations revealed that the stoichiometric formula of cobalt glycerolate corresponds approximately to $CO_{1.3}C_1O_{4.1}H_4$, indicating a higher cobalt content than theoretically expected.

Given complementary insight into the chemical conditions of the elements present. The XPS survey spectrum exhibited clear maxima corresponding to Co 2p, C 1s, and O 1s, confirming the presence of cobalt, carbon, and oxygen as principal components. The Co 2p spectrum displayed characteristic spin–orbit doublets with peaks located at approximately 788.9 eV and 806.9 eV, while the C 1s and O 1s appeared at 284.5 eV and 538.9 eV, accordingly. Minor but discernible features from Co LMM, Co 3s, and Co 3p transitions were also detected, though these were excluded from quantitative evaluation due to their low signal intensity. Based on recalculated compositional ratios, the molecular formula was refined to $CO_{1.8}C_1O_2$, further confirming the cobalt-rich stoichiometry of the precursor. Consistent results were independently verified through AAS measurements, demonstrating excellent agreement between the two analytical techniques.

The outcome of thermal decomposition was found to be highly dependent on the furnace atmosphere during the heating process, in line with the temperature–oxygen partial pressure ($T - pO_2$) phase diagram of the Co–O system for bulk materials. By estimating the oxygen partial pressure (pO_2) from the nitrogen gas purity ($\sim 10^{-7}$), the expected phase equilibria were confirmed experimentally. Under a high-purity nitrogen atmosphere, XRD analysis showed the formation of CoO nanoparticles, whereas in an oxygen-rich environment, Co_3O_4 nanoparticles were obtained. This difference arises from the distinct thermodynamic stabilities of the two phases: while Co_3O_4 is the stable phase under ambient temperature and oxygen-rich conditions, CoO can remain metastable at room temperature due to its nanoscale nature and sluggish oxidation kinetics [41, 42].

XRD patterns of the samples synthesized at 650^oC clearly demonstrated that both CoO and Co_3O_4 products were single-phase materials with well-defined crystalline structures. The experimental diffraction peaks aligned closely with the reference data from standard databases, confirming the phase purity of each sample. The sharpness and strength of the reflections also show successful crystallization during the decomposition process, validating that controlled thermal treatment under tailored gas atmospheres can selectively yield either CoO or Co_3O_4 nanoparticles from cobalt glycerolate precursors.

The dimensions of nanoparticles appear to vary on the reacting heat for both cobalt oxides. This approach therefore proves appropriate for producing Co_3O_4 nanoparticles spanning in dimension from 14.2 to 24.6 nm and CoO nanoparticles that range from 8.4 to 21.6 nm. The tiniest nanoparticles were collected at 450^oC, whereas the biggest were produced at 650^oC.

Additionally, SEM was used to examine the form and diameter size. The corresponding SEM pictures of nanoparticles made at 650^oC are exhibited. These photos are of low grade. Nanoparticles having a diameter of ~ 20 nm are so tiny that their ability to be identified is limited by gadget resolution. Despite this, spherical particles having comparable dimensions may be identified in both cobalt oxides. The TEM pictures corroborated the particle dimensions determined by SEM. Nanoparticles produced at 650^oC were spherical in form and produced agglomerations.

Figure 1 depicts the relationship between light dispersion and CoO particle sizes (16-20 μm). It enhances CoO efficiency by raising wavelength converting efficiency and illumination transmission. To enhance blue-light brightness, forward scattering and reabsorption must be minimized while promoting greater forward-emission dispersion. This improvement is achieved by increasing the particle size of CoO and simultaneously reducing the concentration of yellow phosphor. Figure 2 illustrates that the $YAG : Ce$ yellow phosphor content grows proportionally with CoO dosage. According to Figure 2, enlarging CoO particles (16-20 μm) slightly decreases the

$YAG : Ce$ phosphor ratio from about 27.2% to 27.1%. Figures 3 and 4 indicate that the CCT is largely independent of concentration. Figure 3 further demonstrates that higher doping levels reduce the CCT variation of the phosphor. CCT measurements reveal a peak of approximately 3050K for CoO particles around 19 μm, and a minimum near 3000K for particles of 20 μm. Figure 4 depicts the D-CCT reaching its deepest point of $\sim 47K$ at $19\mu m$ of CoO, approximately $46K$ lower than the maximum value of $\sim 93K$ at $16\mu m$ of CoO.

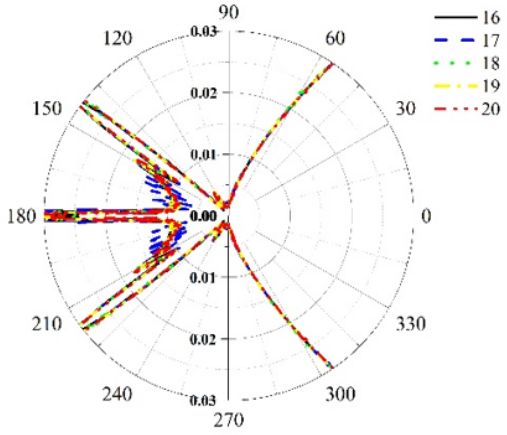

Fig. 1: Scattering factors with various particle sizes.

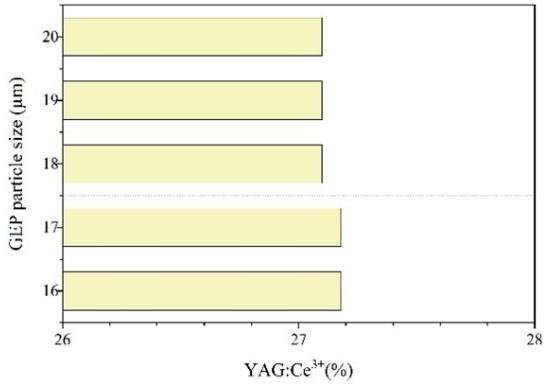

Fig. 2: $YGA : Ce$ phosphor proportion values with different CoO proportions.

Figure 5 shows that CoO does not consistently enhance the brightness of white-light emission. The maximum luminous flux ($\sim$ 73.37 lm) was achieved at a CoO particle dimension of 18 μm,

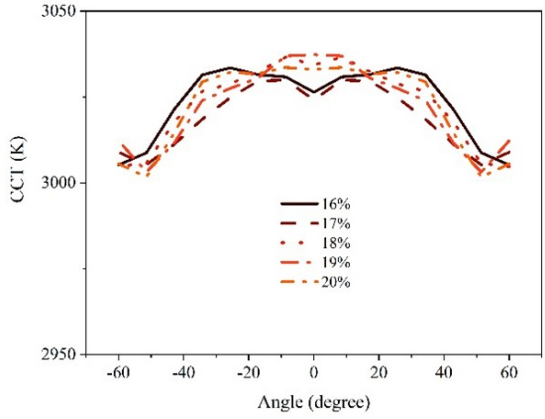

Fig. 3: CCT values with various CoO proportions.

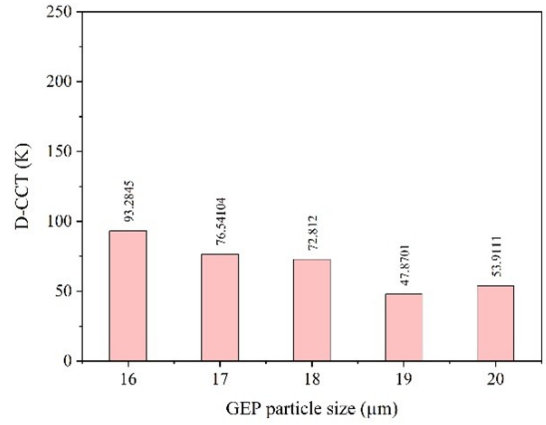

Fig. 4: Color difference values with different CoO proportions.

whereas the lowest value ($\sim$ 73.01 lm) occurred at $16\mu m$. Enhanced backscattering and reabsorption reduce blue emission, leading to nonuniform hue distribution. When larger CoO particles are exposed to stronger backscattered blue light, the phosphor color shifts toward yellow or orange-red. The phosphor covering is effective just within a particular particle-size range, as excessive scattering from surrounding objects induces multiple reflections and narrows the emission spectrum. Consequently, a higher phosphor concentration capably raise the amount of back-reflected changed illumination, resulting in elevated CCT but reduced luminous intensity. As shown in Figure 5, incorporating $18\mu m$ CoO into a simulated WLED yields a luminous performance of approximately 73 lm, thereby en-

hancing both brightness and color uniformity.

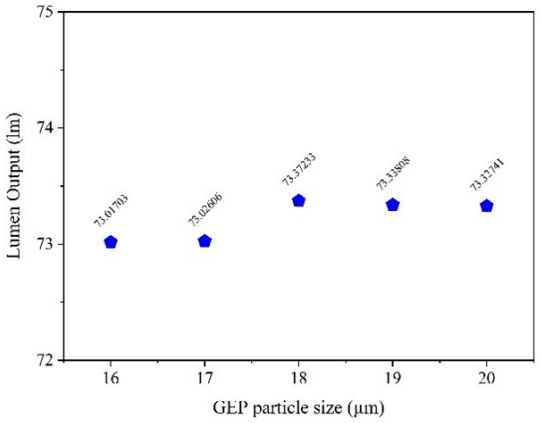

Fig. 5: Luminescence strength with various CoO proportions.

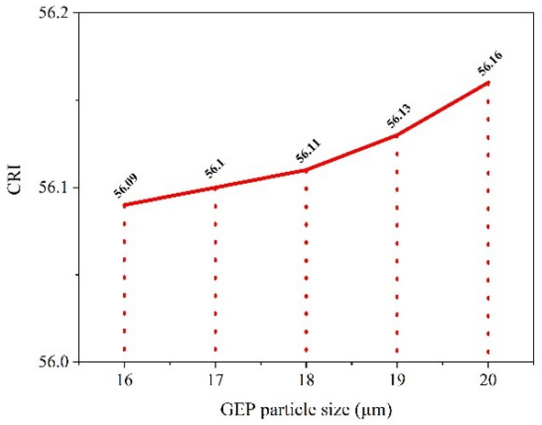

Fig. 6: CRI values with various CoO proportions.

Figures 6 and 7 illustrate the influence of CoO particle size on the brightness and color rendering of white LEDs. The color rendering index (CRI) and color quality scale (CQS) were employed to assess color rendition for particle sizes ranging from 16 to 20μm. A minor increase in CoO particle size resulted in a slight rise in CRI from 56.09% to 56.16% and in CQS from 41.99% to 42.38%. The observed decreases in CRI and CQS at certain conditions may be attributed to the unstable emission behavior of blue, green, and yellow-orange components. Larger CoO particles tend to produce irregular emission patterns, stronger yellow–orange bias, and greater light dispersion. Based on these findings, adjustments to the phosphor's CRI and CQS will

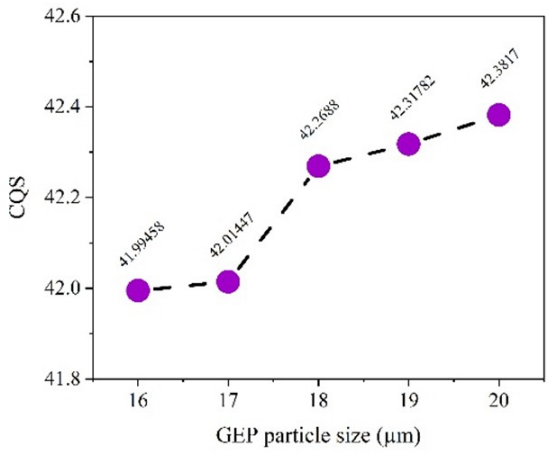

Fig. 7: CQS values with various CoO proportions.

be made, taking into account other influential factors such as particle dimension.

Table 1 summarizes the scattering coefficients of different materials. CoO, reported in this work, shows the lowest scattering coefficient (0.3 mm^{-1}) and reduced scattering coefficient (0.05 mm^{-1}), suggesting weak light-scattering ability. By comparison, SiO_2 exhibits moderate scattering (7.2/0.78 mm^{-1}), while KBr [1] has very strong scattering (42.5/13.5 mm^{-1}). MgO [36] and $CaCO_3$ [41] fall in between, with MgO being weaker (3.54/0.059 mm^{-1}) and $CaCO_3$ showing higher scattering (8.96/0.15 mm^{-1}). These comparisons highlight that CoO functions as a low-scattering material compared to commonly used scatterers. Table 2 compares optical perfor-

Tab. 1: Result comparison of scattering coefficients influenced by particle sizes of scattering materials

Scattering Materials	Scattering coefficients (mm^{-1})	Reduced scattering coefficients (mm^{-1})	References
CoO	0,3	0,05	This work
SiO_2	7.2	0.78	(15)
KBr	42,5	13,5	(1)
MgO	3,54	0,059	(18)
$CaCO_3$	8,96	0,15	(4)

mance in $YAG:Ce^{3+}$-based white LEDs. CoO, as studied here, demonstrates a $YAG:Ce^{3+}$ conversion of 21.18%, CCT of 3000K, and a rel-

atively small ΔCCT of 47.9 K, indicating stable color output. Its CRI (56.16), CQS (42.4), and lumen output (73.3 lm) are similar to those of SiO_2 and KBr, but notably lower in brightness compared with MgO (131.1 lm) and $CaCO_3$ (173.2 lm). However, while $CaCO_3$ achieves the highest luminous flux, it suffers from extremely poor color stability (ΔCCT = 460 K at 6000 K), making it less reliable for uniform lighting.

Overall, these findings underline that CoO offers stable color performance with low scattering and moderate efficiency, making it distinct from higher-scattering, high-lumen materials like $CaCO_3$ and MgO. This stability positions CoO as a potential candidate for applications where consistent color quality is more critical than maximum brightness.

4. Conclusion

The thermally breaking down of cobalt glycerolate provides a flexible approach for synthesizing CoO and Co_3O_4 nanoparticles with controllable particle sizes. This technique offers significant advantages over conventional methods owing to its simplicity, cost efficiency, and capability to produce various forms of cobalt oxide nanoparticles by merely adjusting the thermal parameters and ambient atmosphere. By carefully controlling parameters such as decomposition temperature, oxygen/nitrogen ratio, and heating duration, it is possible to precisely tailor the phase composition and size distribution of the outcome nanoparticles. Further optimization, for example through the use of fluidized furnaces or the introduction of inert additives, can enhance the uniformity and isolation of individual nanoparticles, minimizing aggregation and improving reproducibility. Cobalt-based nanoparticles produced in this way exhibit a wide range of functional properties, making them highly suitable for applications in lithium-ion batteries, gas sensors, catalysis, supercapacitors, and other nanoelectronic devices, where their unique structural, magnetic, and electrochemical characteristics can be fully leveraged.

5. Acknowledgements

The authors wish to express their gratitude to the Posts and Telecommunications Institute of Technology, Vietnam, for financial support for this research.

References

[1] N.D.Q. Anh, N.T.P. Loan, P.V. De, and H.Y. Lee. Potassium bromide scattering simulation for improving phosphor-converting white led performance. *Optoelectron. Adv. Mater. - Rapid Commun.*, 19(7-8):378–383, 2025.

[2] M. Naeem, A. Yaqoob, T. Iqbal, J. Iqbal, J. C. Diaz Guillén, S. Nazer, and J. D. Elizondo. Synthesis of cobalt oxide nanoparticles by atmospheric pressure microplasma and their structural, optical, antifungal and antibacterial properties. *BioNanoScience*, 15(1):26, 2024.

[3] M. H. N. Thi, N. T. P. Loan, and N. D. Q. Anh. Study of red-emitting laaso4:eu3+ phosphor for color rendering index improvement of WLEDs with dual-layer remote phosphor geometry. *Telecommun. Comput. Electron. Control.*, 18(6):3210, 2020.

[4] H. T. Tung, N. D. Q. Anh, and H. Y. Lee. Impact of phosphor granule magnitudes as well as mass proportions on the luminous hue efficiency of a coated white light-emitting diode and one green phosphor film. *Optoelectron. Adv. Mater. - Rapid Commun.*, 18(1-2):58–65, 2024.

[5] N. D. Q. Anh. Nano scattering particle: an approach to improve quality of the commercial led. *J. Sci. Technol.*, 22(3):53–57, 2024.

[6] Q. Dai, C. Duty, and M. Z. Hu. Semiconductor-nanocrystals-based white light-emitting diodes. *Small*, 6(15):1577–1588, 2010.

[7] H. Fujii, H. Sakurai, K. Tani, L. Mao, K. Wakisaka, and T. Hirao. Vivid-

Tab. 2: Result comparison of scattering coefficients influenced by particle sizes of scattering materials

Scattering Materials	YAG:Ce^{3+} (%)	CCT (K)	DCCT (K)	CRI	CQS	Lumen (lm)	References
CoO	21,18	3000	47,9	56,16	42,4	73,3	This work
SiO_2	27,4	3000	30	56.3	42.5	73.7	(15)
KBr	27,4	3000	35,4	56,2	42,4	73,7	(1)
MgO	14,5	4000	53,6	58,2	64,2	131,1	(18)
$CaCO_3$	5,95	6000	460	60,8	62,6	173,2	(4)

red and highly efficient phosphors bearing diphenylquinoxaline units and their application to organic light-emitting devices. *Int. Meet. for Future Electron Devices*, 12:35–36, 2004.

[8] S. Goswami, S. Chakravarty, M. Chakraborty, and D. De. Exchange interaction in metal oxides core-shell nanoparticles Co_3O_4-CoO. *Indian J. Phys.*, 99:1033–1040, 2024.

[9] C. Guo, L. Luan, Y. Xu, F. Gao, and L. Liang. White light–generation phosphor $Ba_2Ca(BO_3)_2 : Ce^{3+}, Mn^{2+}$ for light-emitting diodes. *J. Electrochem. Soc.*, 155(11):J310, 2008.

[10] A. Herrmann, D. Friedrich, T. Zscheckel, and C. Russel. Luminescence properties of sm^{3+} doped alkali/earth alkali orthoborates of the type $XZBO_3$ with $X = Li, Na, Cs$ and $Z = Ca, Sr, Ba$. *J. Lumin.*, 214:116550, 2019.

[11] W. T. Hong, J. Lee, H. I. Jang, S. J. Park, J. S. Joo, and H. K. Yang. Orange-red light emitting europium doped calcium molybdate phosphor prepared by high energy ball milling method. *20th Microoptics Conf. (MOC)*, pages 1–2, 2015.

[12] M. Huang, X. Yang, and F. Jiang. Dielectric and luminescent properties of sm^{3+} doped $Ba(Zn1/3Nb2/3)O3$ ceramics with perovskite structure. *Mater. Res. Express*, 5(6):066301, 2018.

[13] S. Jayakiruba, S. S. Chandrasekaran, P. Murugan, and N. Lakshminarasimhan. Excitation-dependent local symmetry reversal in single host lattice $Ba2A(BO3)2 : Eu3+$[A = Mg and Ca] phosphors with tunable emission colours. *Phys. Chem. Chem. Phys.*, 19(26),:17383–17395, 2017.

[14] J. E. Murphy, W. W. Beers, M. D. Butts, S. J. Camardello, A. Chowdhury, W. E. Cohen, and A. Setlur. Narrow band emitting LED phosphors for wide color gamut displays & energy efficient ssl. *IEEE Photonics Conf. (IPC)*, pages 1–1, 2018.

[15] Y. Peng, H. Cheng, Z. Chen, and R. Li. Multi-layered red, green, and blue phosphor-in-glass for ultraviolet-excited white light-emitting diodes packaging. *17th Int. Conf. on Electron. Packag. Technol. (ICEPT)*, pages 61–64, 2016.

[16] M. Saito and H. Kondo. Battery-independent emergency illumination with RGB phosphors. *Proc. 39th Annu. 2005 Int. Carnahan Conf. on Secur. Technol.*, page 222–225, 2005.

[17] C. Shao, Z. Peng, B. Yu, Z. Li, and X. Ding. The detail study on the effect of the flow during the curing process of phosphor particles on the color performance. *21st Int. Conf. on Electron. Packag. Technol. (ICEPT)*, pages 1–4, 2020.

[18] P. Shao, P. Xiong, Y. Xiao, Z. Chen, D. Chen, and Z. Yang. Self-recoverable nir mechanoluminescence from $Cr3+$ doped perovskite type aluminate. *Adv. Powder Mater.*, 3(2):100165, 2024.

[19] C. Shen, K. Li, Q. Hou, H. Feng, and X. Dong. White LED based on YAG : CE,GD phosphor and CDSE–ZNS core/shell quantum dots. *IEEE Photonics Technol. Lett.*, 22(12):884–886, 2010.

[20] C. Shen, C. J. Zhong, K. Li, and J. Ming. High color rendering index wled based on $YAG : Ce < sup > 3+ < /sup >, Gd < sup > 3+ < /sup >$ nano-phosphor. *Asia Commun. Photonics Conf. Exhib.*, 2010.

[21] J.-K. Sheu, S. J. Chang, C. Kuo, Y. Su, L. Wu, Y. Lin, and R. Wu. White-light emission from near UV InGaN-GaN LED chip precoated with blue/green/red phosphors. *IEEE Photonics Technol. Lett.*, 15(1):18–20, 2003.

[22] H.-K. Shih, C.-N. Liu, W.-C. Cheng, and W.-H. Cheng. Phosphor-in-glass for high performance wleds by reduction phosphor interaction and AR coating. *IEEE Photonics Technol. Lett.*, 33(20):1143–1146, 2021.

[23] C.-C. Tsai. Thermal aging performance analyses of high color rendering index of glass-based phosphor-converted white-light-emitting diode. *IEEE Trans. on Device Mater. Reliab.*, 15(4):617–620, 2015.

[24] S. D. Ho, N. T. P. Loan, H.-Y. Lee, and N. D. Q. Anh. Study of $K_2siF_6 : mn^{4+}@siO_2$ phosphor for white LEDs with high angular color uniformity. *J. Adv. Eng. Comput.*, 8(1):53–62, 2024.

[25] C. Moya, A. Rodríguez, J. Sánchez, and A. Vázquez. Characterization of cobalt oxide nanoparticles prepared by the thermal decomposition. *J. Nanostructure Chem.*, 4:33, 2014.

[26] A. C. Pereira, A. L. Magalhaes, I. S. Gonçalves, and A. M. Silva. Simple preparation of ferromagnetic Co_3O_4 nanoparticles by thermolysis of the $Co(NH_3)_{62}$ complex. *SpringerPlus*, 3:16, 2014.

[27] D. Gutiérrez-Martín, A. Sagastume, E. Blanco, and A. Pereira. Revisiting the decomposition process of tetrahydrate Co(II) acetate. *Appl. Sci.*, 12(13):6786, 2022.

[28] J. Kießling, S. Rosenfeldt, and A. S. Schenk. Size-controlled liquid phase synthesis of colloidally stable Co_3O_4 nanoparticles. *Nanoscale Adv.*, 5:3942, 2023.

[29] D Das and B. J. Saikia. Synthesis, characterization and biological applications of cobalt oxide (Co_3O_4) nanoparticles. *Chem. Phys. Impact*, 6:100137, 2022.

[30] V. R. Balaji, M. A. I. Jahan, G. K. Bharti, A. Yadav, and R. V. Honnungar. Fbg sensor applications in aerospace engineering. *Adv. Opt. Sensors for Aerosp. Appl.*, 37:97–123, 2024.

[31] M. Salavati-Niasari, N. Mir, and F. Davar. Synthesis and characterization of Co_3O_4 nanorods by thermal decomposition of cobalt oxalate. *J. Phys. Chem. Solids*, 70(5):711–718, 2009.

[32] J. Kießling, S. Rosenfeldt, and A. S. Schenk. Size-controlled liquid phase synthesis of colloidally stable Co_3O_4 nanoparticles. *Nanoscale Adv.*, 5:3942–3950, 2023.

[33] S. Farhadi and J. Safabakhsh. Solid-state thermal decomposition of the $[Co(NH_3)_5CO_3]NO_30.5H_2O$ complex: a simple, rapid and low-temperature synthetic route to Co_3O_4 nanoparticles. *J. Alloy. Compd.*, 515:180–185, 2012.

[34] N. T. P. Loan and N. D. Q. Anh. The effects of zno particles on the color homogeneity of phosphor-converted high-power white LED light sources. *Int. J. Electr. Comput. Eng.*, 10(5):5155, 2020.

[35] A.-M. D. Tran, N. D. Q. Anh, and N. T. P. Loan. Enhancing light sources color homogeneity in high-power phosphor-based white LED using Zno particles. *Telkomnika,*, 18(5):2628, 2020.

[36] N. T. P. Loan and N. D. Q. Anh. Utilizing $CaCO_3$, CaF_2, SiO_2, and TiO_2 particles to enhance color homogeneity. *Int. J. Electr. Comput. Eng.*, 10(5):5175, 2020.

[37] M. H. N. Thi, N. T. P. Loan, and N. D. Q. Anh. Improving optical properties of remote phosphor led using green $Y_2O_3 : Ho^{3+}$

and red $Mg_4(F)(Ge, Sn)O_6 : Mn^{2+}$ layers. *Telkomnika*, 18(6):3228, 2020.

[38] M. H. N. Thi, P. T. That, and N. D. Q. Anh. Eu^2+ activated strontium-barium silicate: a positive solution for improving luminous efficacy and color uniformity of white light-emitting diodes. *Mater. Sci.*, 38(4):594, 2020.

[39] V. T. Pham, N. H. Phan, G.-F. Luo, H.-Y. Lee, and D. Q. A. Nguyen. The application of calcium carbonate $CaCO_3$ and Titania TiO_2 for color homogeneity and luminous flux enhancement in PC-LEDs. *J. Adv. Eng. Comput.*, 5(2):75–82, 2021.

[40] H. T. Tung, M. H. N. Thi, and N. D. Q. Anh. Improved color uniformity in white light-emitting diodes using LiLu(MoO4)2:Sm3+ combined Sio2 composite. *Int. J. Technol.*, 15(1):8, 2024.

[41] H. T. Tung, B. T. Minh, N. L. Thai, H. Y. Lee, and N. D. Q. Anh. Zno particles as scattering centers to optimize color production and lumen efficiencies of warm white LEDs. *Optoelectron. Adv. materials - rapid communications*, 18(5-6):1–6, 2024.

[42] P. H. Cong, L. X. Thuy, N. T. P. Loan, H. Y. Lee, and N. D. Q. Anh. ZnO-doped yellow phosphor compound for enhancing phosphor-conversion layer's performance in white leds. *Optoelectron. Adv. materials – rapid communications*, 18(7–8):389, 2024.

About Authors

Nguyen Thi Phuong LOAN was born in Da Nang province. In 2006, She received her master degree from University of Natural Sciences. She received her PhD degree from Ton Duc Thang University in 2024. Her research interest is optoelectronics. She has worked at the Faculty of Fundamental 2, Posts and Telecommunications Institute of Technology, Ho Chi Minh City, Vietnam. She can be contacted at email: ntploan@ptithcm.edu.vn.

Hsin-Yi MA was born in Hsinchu city, Taiwan. She has been working at the Department of Industrial Engineering and Management, Minghsin University of Science and Technology, Hsinchu, Taiwan. Her research interest is Production optimization and Optics.

Hsiao-Yi LEE was born in Hsinchu city, Taiwan. He has been working at the Department of Electrical Engineering, National Kaohsiung University of Science and Technology, Kaohsiung, Taiwan. His research interest is optics science. He can be contacted at email: hsiaoyi.nuk@gmail.com.